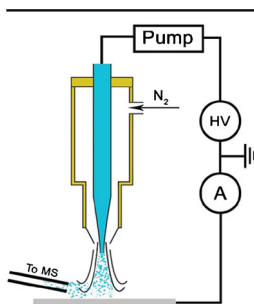


RESEARCH ARTICLE

Probe-Substrate Distance Control in Desorption Electrospray Ionization

Tyler J. Yarger, Elizabeth M. Yuill, Lane A. Baker

Department of Chemistry, Indiana University, 800 E. Kirkwood Ave., Bloomington, IN 47405, USA



Abstract. We introduce probe-substrate distance (D_{ps})-control to desorption electrospray ionization (DESI) and report a systematic investigation of key experimental parameters. Examination of voltage, flow rate, and nebulizing gas pressure suggests as D_{ps} decreases, the distance-dependent spray current increases, until a critical point. At the critical point the relationship inverts, and the spray current decreases as the probe moves closer to the surface due to constriction of solution flow by the nebulizing gas. D_{ps} control was used to explore the use of spray current as a signal for feedback positioning, while mass spectrometry imaging was performed simultaneously. Further development of this technique is expected to find application in study of structure-function relationships for clinical diagnostics, biological investi-

gation, and materials characterization.

Keywords: DESI, MSI, Surface, Imaging

Received: 17 August 2017/Revised: 3 November 2017/Accepted: 3 November 2017/Published Online: 27 November 2017

Introduction

Desorption electrospray ionization (DESI) has received significant attention as an ambient mass spectrometry ionization technique, with a wide variety of experimental configurations [1, 2]. DESI typically involves application of several kilovolts of potential to a solution within a capillary to generate electrospray. The spray capillary is placed coaxially inside a second capillary, which delivers a shroud of nebulizing gas to direct electrosprayed droplets towards a surface of interest. As electrosprayed droplets impact the surface, a thin liquid film of solution is formed and analyte present on the surface is desorbed [3, 4]. Upon further bombardment of electrosprayed droplets, secondary droplets that contain analyte can be liberated from the thin film. Secondary droplets are then desolvated, and the analytes are ionized as the droplets are carried to a mass spectrometer for analysis via a transfer line [3, 5–12]. The spray capillary can be rastered across the substrate to perform ambient mass spectrometry imaging (MSI). Present DESI configurations scan at constant height, which may present challenges in convolution of chemical signal over samples with varied topography. Additionally, ability to dynamically respond to variations in height may eliminate sample preparation steps (e.g., slicing tissue into flat sections), and collection of topographic information may be useful for understanding sample morphology.

Herein, we characterize interactions between the electrospray emitter and surface via a probe-substrate distance (D_{ps}) measurement, with a goal to develop a signal suitable for dynamic feedback to allow for topographic imaging, which may ultimately expand applications of DESI and MSI.

In recent work, a shear force probe, which is used to provide probe-substrate distance control, has been incorporated with nanoDESI [13]. This DESI-variant differs from traditional DESI operation, as a liquid junction between two capillaries is used to desorb analytes and transfer solution to a MS, rather than droplets propelled by a nebulizing gas [14]. Moreover, the size of the liquid contact determines imaging spatial resolution. Typical DESI methods, which utilize nebulizing gas, to date have not recorded topography. Herein we explore the possibility to simultaneously obtain topographic and DESI-MSI information.

We have recently introduced scanning electrospray microscopy (SESM) as a new method to control the distance between the tip of a electrospray emitter and a surface of interest [15]. SESM is operated by application of a potential to a pipette filled with conductive solution to generate electrospray over a substrate. As the pipette is moved towards the surface via a piezoelectric positioner in SESM, distance-dependent current rapidly increases. Current values are recorded as the SESM pipette approaches the surface until a predefined current (set point) is reached, at which point the extension distance of the piezoelectric positioner is recorded. The pipette is then retracted to the original starting point, moved laterally to the

next pixel, and the approach-retract process repeated to build a topographic image of the surface [16].

In this report, we describe the first steps to SESM-DESI, which combines the positioning and feedback of SESM with chemical imaging capabilities of DESI to provide a method that collects spatial (x, y, z) information correlated with mass spectrometric data. SESM-DESI approach curves are recorded with incorporation of the additional components necessary for DESI (nebulizing gas and backing syringe pump), as depicted in Figure 1a. The influence of voltage, flow rate, and gas pressure are systematically evaluated as a function of probe-substrate distance. While there are some combined topography/MSI techniques (e.g., AFM/MSI from the Van Berkel group) [17, 18], ambient spray-based techniques present an advantage in that they are potentially less destructive to the sample and are non-contact in nature, while still enabling soft ionization. Moreover, imaging via DESI at a constant probe-surface distance would prevent convolution due to variations in sample height [19]. Careful tuning of these experimental parameters was performed on synthetic samples; however, once developed, SESM-DESI is intended to enable elucidation of structure-function relationships on materials such as non-sectioned tissue samples, biofilms, and patterned surfaces.

Experimental

Materials

The following chemicals and materials were used as received: anhydrous methanol (Avantor, Center Valley, PA, USA), formic acid 90% (Mallinckrodt, Phillipsburg, NJ, USA), Milli-Q water (18.2 M Ω -cm, Millipore Corp., Danvers, MA, USA), rhodamine 6G (Sigma-Aldrich, St. Louis, MO, USA),

nitrogen gas (UHP, Airgas, Radnor, PA, USA). Spray solution for all experiments described consisted of (50:50:0.1 MeOH/H₂O/HCOOH). Rhodamine 6G was dissolved in methanol to a concentration of 10 mM.

Pipette Fabrication

Borosilicate pipettes (B100-58-10, Sutter Instrument, Novato, CA, USA) that measure 10 cm in length \times 1.0 mm outer diameter (o.d.) \times 0.58 mm inner diameter (i.d.) were pulled with a P-2000 pipette puller (Sutter Instrument). Pulled pipettes were then microforged (F-500, Technical Products International, St. Louis, MO, USA) to an i.d. of \sim 10 μ m.

Probe Fabrication

A pipette holder, 4 cm in length, was constructed from four parts (Figure 1a, labeled A–D). An end cap with a 1.1 mm hole (part A) was attached to the end of the holder, and the back end of the pipette was pushed through this hole and attached to an infusion line. A rubber septum was placed inside the end cap to seal any gaps. The center body of the pipette holder (part B) contained a welded 1/8" Swagelok inlet, removed from a union tee (SS-100-3, Swagelok, Indianapolis, IN, USA) to serve as a nitrogen gas inlet. Within part B was a metal septum, pictured in Figure 1c, with half of the material removed, to allow air flow around the pipette while keeping the pipette centered. The bottom of the probe (part C) consisted of a detachable hollow cylinder to which the nebulizing tip (part D) was attached.

To secure the nebulizing tip to the bottom of the probe a larger \sim 250 μ m i.d. pipette was scored with a diamond stylus at the shoulder of the pipette. The pipette was back-inserted into the probe holder and positioned so that \sim 3 mm of the pipette protruded from the pipette holder. The pipette was then secured

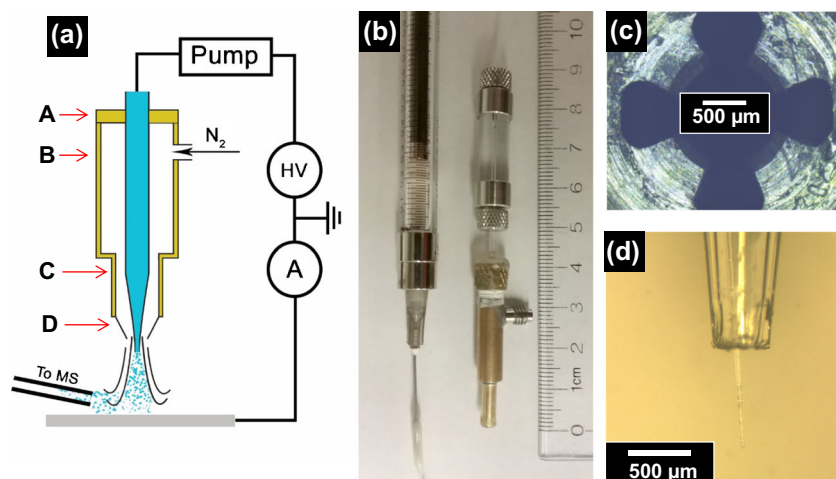


Figure 1. (a) Schematic, not drawn to scale, that depicts the basic setup of the probe holder and instrumental setup of SESM-DESI. Parts labeled A, B, C refer to the brass end cap, center body, and lower body respectively. Part D represents the nebulizing nozzle formed from a pipette tip. Secondary droplets are transferred to the mass spectrometer via a Tygon tubing inlet. (b) Image of probe holder loaded with a pipette. The pipette is connected to the syringe via a union and PTFE tubing. (c) The inside of the pipette holder (part B), not shown in Figure 1a. The partial septum holds the pipette in place and aligned while nebulizing gas is allowed to pass through the chamber. (d) Close-up image of the spray pipette that protrudes past the nebulizing tip. The distance between the inner pipette tip and outer nebulizing tip is referred to here as the tip-protrusion distance

to part C with a thin epoxy seal. The pipette was then cleaved at the scored position, which left a nebulizing tip intact that was naturally centered in the pipette holder. The electrospray emitter was then inserted into the pipette holder from part B, part C was attached to the probe, and the emitter was forced through part D so that the emitter tip protruded from the nebulizing tip by ~ 0.5 – 1 mm. A small amount of epoxy or hot glue was placed at the end cap to further prevent the loaded pipette from moving.

Sample Preparation

Transmission electron microscopy (TEM) grids (12410-Cu, Ted Pella Inc., Redding, CA, USA) were prepared by first drop-casting 10 mM rhodamine 6G solution onto the grid, then air drying. Coated grids were then secured onto a stainless steel substrate via carbon tape (Nisshin EM Co., Ltd., Tokyo, Japan). Known TEM grid dimensions were determined via the manufacturer and confirmed with a stylus profilometer (KLA-Tencor P-7, Milpitas, CA, USA), imaged at $100 \mu\text{m/s}$ with 1 mg-force. Whatman paper (1001-055, Whatman International, Maidstone, England) was sputter-coated (Denton Vacuum LLC., Moorestown, NJ, USA) for 60 s at 28 mA to create an absorbent, conductive substrate.

Instrument Setup

Coarse probe positioning was achieved by mounting x , y , z (defined as forwards/backwards, left/right, up/down, respectively) micromanipulators (460 Series, Newport Corp., Irvine, CA, USA) onto a bridge over an inverted microscope (Nikon Diaphot, Tokyo, Japan). A 15 mm full range stepper motor (M-111.1DG, Physik Instrumente, Karlsruhe, Germany) was fastened to the z -positioner. A Teflon mount was used to attach the probe to the stepper motor.

Coarse sample positioning was controlled by y and z micromanipulators, whereas a second 28 mm stepper motor (Zaber Tech., Vancouver-BC, Canada) controlled the x -axis. Samples of interest were placed onto an L-bracket (sample mount), which was attached to the z -micromanipulator.

When imaging, the x and z axes were automated with the two stepper motors controlled via LabVIEW, with the y -axis controlled by hand via a micromanipulator. Current at the substrate was measured with a Keithley 414S picoammeter (Keithley Instruments, Cleveland, OH, USA). Signal from the Keithley was input to LabVIEW and served as the positioning feedback signal. A 1 mL gas-tight syringe (Hamilton, Reno, NV, USA) was fitted with a 22 gauge needle (BD Precision Glide, Franklin Lakes, NJ, USA), which was connected to the pipette via PTFE tubing (Cole-Parmer, Vernon Hills, IL, USA). Flow rates were controlled by a syringe pump (NE-1600, New Era Pump Systems, Farmingdale, NY, USA). A 5 kV DC power supply (Fisons Instruments, Ipswich, UK) was attached to the metal needle in contact with spray solution to achieve electrospray. Nitrogen gas was connected to the pipette holder gas inlet via PTFE tubing. Tygon tubing, $1/8'' \times 1/16'' \times \sim 1$ m long, was used to transfer the resultant ions to a Bruker

MicrOTOF mass spectrometer (Bruker, Billerica, MA, USA). A 10 cm stainless steel inlet adapted the transfer line to the mass spectrometer.

Data Collection and Processing

Topographic data was exported from LabVIEW and was processed in Origin. Zeroing of the z -axis was performed by approaching the surface with application of ~ 1 – 10 V to the probe in the absence of nebulizing gas and with no infusion. Once the meniscus made contact with the sample surface, the circuit completed and a nonzero current was read, similar to scanning electrochemical cell microscopy (SECCM) [20]. Determination of this point, where $D_{ps} = 0$, provided a reference point for subsequent SESM approach and imaging experiments, such that the actual distance above a surface could be determined.

Imaging was performed with a variant of approach-retract scanning mode (S-1) [16]. First the probe was positioned $\sim 650 \mu\text{m}$ from the surface, as determined from SECCM. A 5 V trigger was produced through LabVIEW and sent to the MS to initialize/synchronize the MS. The timed master loop (which controlled probe positioning) was then initialized as the probe was approached to the surface, first by a single coarse $500 \mu\text{m}$ step, then followed by several $2 \mu\text{m}$ steps (fine approach). The probe stopped and recorded the height of the stepper motor once the current decreased to a predetermined set point value of 1 nA. The probe was then retracted by $550 \mu\text{m}$ and held in place until a loop time of 5 s had expired, which completed one iteration of the loop. The loop time is user-defined and was chosen to ensure the program finished prior to acquisition of a new measurement by the MS. The approach/retract cycle takes ca. 2–3 s, thus a 5 s loop was chosen to allow an adequate buffer before taking a new measurement with the MS. The sample was then moved forward, via the stepper motor, one step ($100 \mu\text{m}$) in the x -direction and the probe was brought $500 \mu\text{m}$ towards the surface to start a new approach. Positions of the probe were recorded at the end of every fine approach once the current reached the set point of 1 nA. After one line scan was completed, another 5 V trigger stopped the mass spectrometer. The probe was returned to the initial x and z positions, and the sample mount was manually moved one step laterally in the y -direction via the micromanipulator.

Mass spectrometry data compiled to make an image was acquired as one line per file. The resultant total ion chromatograms were exported in .mzXML format and converted to .mzML with MSConvert [21], ImzML Convert [22] was then used to combine the .mzML files into a single .imzML file, which was processed in MSiReader [23] to generate an image.

Topography and mass spectrometry images were temporally co-registered by setting the mass spectrometer integration time and the probe-control loop in LabVIEW to equal times (5 s). With this imaging routine, the topography and chemical images in Figure 6 were acquired in ~ 40 min. for an area of 5.1 mm^2 and a pixel size of $100 \times 100 \mu\text{m}$. Vertical resolution with the employed stepper motor is $2 \mu\text{m}$.

Results and Discussion

To achieve maximum utility, chemical information provided by DESI-MSI can be combined with topography information, such as that obtained by several scanning probe microscopy techniques. We have recently described SESM [15], where the basis of probe-substrate interaction is the distance-dependent spray current, which is recognized in the Pfeifer and Hendricks approximation [24] (Eq. 1) and distance-dependent electric field equation [25] (Eq. 2). Briefly, spray current (I) is dependent on several constants, which include solvent permittivity (ϵ), surface tension of the solvent (γ), the permittivity of vacuum (ϵ_0), as well as the conductivity (K), the electric field between the emitter and substrate (E), and the flow rate (V_f). Substitution of Eq. 2 into Eq. 1 further implies the spray current is a function of the potential applied (V_c) between the emitter and substrate, the radius of the pipette (r_c), the spray distance (d), and a constant (A) [26, 27]. From this example, the electric field is proportional to the inverse of $\ln(d)$, electro spray current is approximated to have an exponential-like distance relationship as shown in Figure 2.

$$I = \left[(4\pi/\epsilon)^3 (9\gamma)^2 (\epsilon_0)^5 \right]^{1/7} [KE]^{4/7} [V_f]^{3/7} \quad (1)$$

$$E_c = \frac{AV_c}{r_c \ln(4d/r_c)} \quad (2)$$

To understand differences between DESI and SESM, experimental conditions must be considered. For example, nebulizing gas must be employed in DESI to transfer the liquid film on the substrate to the MS. With addition of nebulizing gas to the

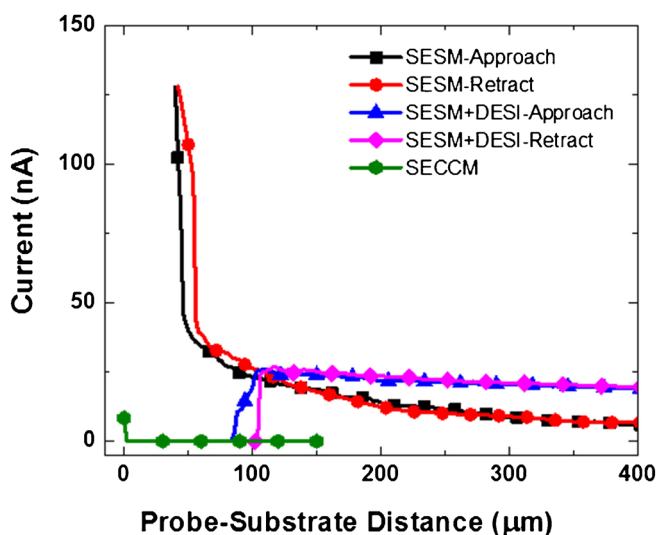


Figure 2. Approach and retract curves over sputter coated Whatman paper taken without the use of nebulizing gas or a syringe pump (SESM) and then with 160 psi nebulizing gas and 2 $\mu\text{L}/\text{min}$ flow rate (SESM+DESI) from a 10 μm i.d. pipette held at 650 V. A pseudo-SECCM approach is also shown to illustrate how the zero point probe-substrate distance was determined

SESM experimental setup, the general trend of exponentially rising current with decreased D_{ps} in SESM is lost (Figure 2, SESM+DESI traces). Instead, as the probe is approached to the surface, an initial increase in current was observed until the probe reached a maximum current (typically $\sim 100 \mu\text{m}$ from the surface), at which point the current either (1) decreased or (2) fell to zero. The observed decrease in current during SESM approach is only observed when nebulizing gas is employed. One possible explanation is that the stream of electrosprayed solvent is constricted by the force of the sheath nebulizing gas; an effect which may be compensated with an increase in solvent flow rate, described further *vide infra*. This decrease in current was found to be highly reproducible (S-2), and was suitable for use as the signal for feedback-based, distance-dependent imaging. A feedback set point of 1 nA was chosen due to close proximity (2 μm away) to the reproducible zero point.

A series of experiments were performed to examine the influence of voltage, flow rate, and nebulizing gas pressure on the approach curve shape and the magnitude of spray current. A geometry-independent configuration [28] (i.e., 90° spray angle) was used to ensure the spray spot on the substrate did not translate across the surface as the probe approached and retracted vertically, although this does present a trade-off between topographic spatial resolution and decreased DESI sensitivity, relative to traditional angled-DESI geometries.

Voltage Influence on Approach Curve Shape and Current

Typically, DESI experiments are performed with emitters of radii $\sim 25 \mu\text{m}$ and spray heights of 2–5 mm, which often requires application of several kV to the emitter. Studies presented herein, however, employ smaller probes (5 μm radius) and shorter probe-substrate distances (~ 100 –500 μm), which allow for voltages in the range of 500–1000 V for generation of electrospray. Typical electrospray onset potentials at 500 V were observed in the absence of nebulizing gas. Experiments described here used a stainless steel conductive substrate from which the current was monitored. Although this configuration of SESM necessitates a conductive surface to measure current and to support electrospray onset, imaging of insulative features on a conductive surface has been demonstrated [15]. We expect substrates with small regions of non-conductive features could be imaged, given that the region is not significantly larger than the electrospray spot size; however, herein we employ a conductive surface to simplify parametric development of SESM-DESI.

Current-voltage (I-V) curves (Figure 3a) were performed with the SESM-DESI experimental setup, with a constant nebulizing pressure and probe-substrate distance at different solution flow rates (1–20 $\mu\text{L}/\text{min}$). For conditions tested, current-voltage curves showed a linear-ohmic relationship, which did not change with flow rate. Application of potentials outside of the 500–1000 V range often yielded sporadic currents; the former may be the result of operation below the onset potential in the case of voltages below 500 V. A series of approaches were performed at three different voltages, each of which was tested at two different

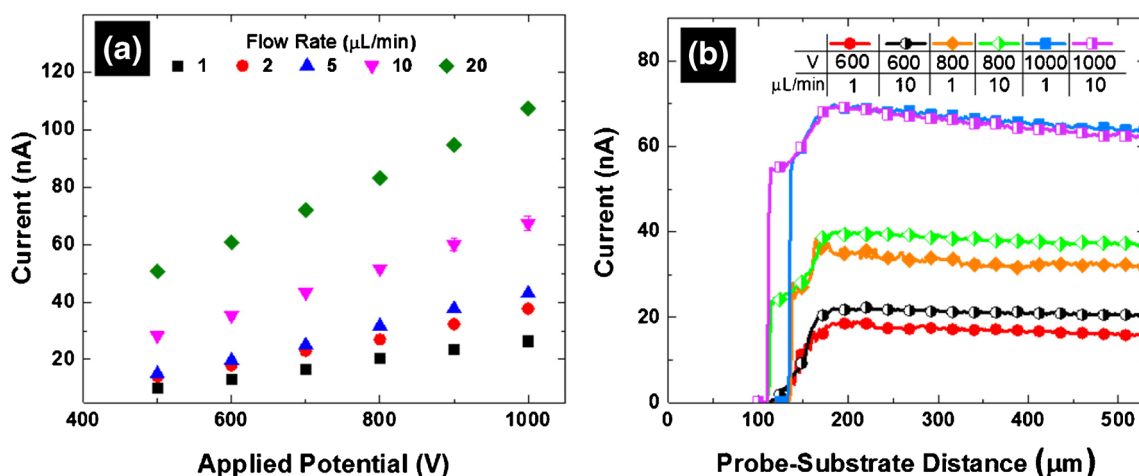


Figure 3. (a) I-V curves taken, in triplicate, at a constant probe-surface distance of 200 μm , under a constant nebulizing pressure of 160 psi with a 10 μm i.d. pipette. An ohmic relationship was observed with all R^2 values >0.995 . (b) Approaches taken with a 10 μm pipette at 600, 800, 1000 V applied potential and at solution flow rates of 1 and 10 $\mu\text{L}/\text{min}$ under a constant nebulizing pressure of 150 psi

solution flow rates (Figure 3b). When solution flow rate was kept constant, alteration of the voltage did not influence the approach curve shape; the current began to decrease and reached 0 nA at the same probe-substrate distances for different voltages. Voltage was only found to increase the magnitude of the current. Because the voltage parameter does not influence the probe-substrate interaction to a significant degree, voltage was the last parameter that was tuned when setting up an experiment, and was adjusted until the current fell in the range of ~ 10 – 30 nA.

Flow Rate Influence on Approach Curve Shape and Current

Prior to acquiring solution flow rate data, the system was equilibrated for 5 min after the solution flow rate was altered. Electro spray current was measured at varied solution flow rates while probe-substrate distances of either 100 or 260 μm were maintained (Figure 4a). Comparison of currents in Figure 3a and Figure 4a suggests variation of applied voltage influenced

the magnitude of current more than solution flow rate. More importantly, a change in the shape of the approach curve was observed when the solution flow rate was altered (Figure 4b). Approaches with larger flow rates, such as 2 or 5 $\mu\text{L}/\text{min}$, showed a current minima near the substrate, but never reached 0 nA. However, approaches with lower flow rates (e.g., 0.5 $\mu\text{L}/\text{min}$) did result in a declining current that reached zero nA. For the example shown in Figure 4b, the switch in approach curve shape occurred between 0.5 and 2 $\mu\text{L}/\text{min}$; however, alterations in experimental conditions (pipette size/geometry, protrusion distances, pressures) resulted in changes in approach curve shape occurring at different flow rates.

Zero-value currents can be explained through consideration of forces that act on the flow of solution. When solution flow rates are sufficiently low, the force of the syringe pump that pushes the solution from the pipette cannot overcome the force of the nebulizing gas constricting flow on the pipette, thus causing spray to stop. As the solution flow rate increases, the

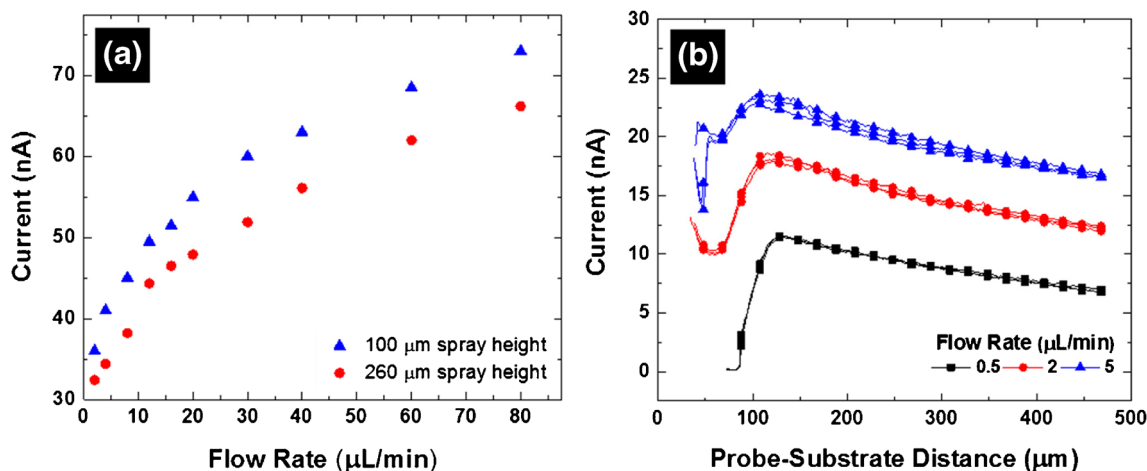


Figure 4. (a) Current dependence of flow rate acquired at two different probe-substrate distances. (b) Approach curves taken in triplicate at 0.5, 2.0, 5.0 $\mu\text{L}/\text{min}$ flow rates with a 10 μm pipette under a constant nebulizing pressure of 150 psi

force of the syringe pump can become sufficient to overcome the force of the nebulizing gas so that flow of solvent from the pipette is only slightly hindered, which yields a decrease in current without completely stopping flow. The decrease in current is further verified by investigation of the influence of nebulizing pressure that acts on the pipette opening (vide infra).

Nebulizing Gas Pressure Influence on Approach Curve Shape

The final parameter examined was nebulizing gas pressure, as measured from the external gas supply. No reproducible trend was observed when current was measured as a function of nebulizing pressure with all other conditions held constant. We have observed current below the electrospray onset potential, as determined in the absence of nebulizing gas and infusion, and attribute the observation of current to the flow of solvent due to Venturi assistance and infusion. As a result, the need for an electrospray onset potential was not required to measure current. Similar observations have been reported before in electrosonic spray ionization, where high velocity nebulizing gas supports spray at potentials below electrospray onset, which can be used for gentler ionization [29]. In these studies, experiments were not performed below the electrospray onset voltage, as determined prior to imaging in the absence of nebulizing gas and infusion.

The influence of pressure on the approach shape is shown in Figure 5. Like Figure 4b, change in the characteristic response of the approach curve is observed, with curves that demonstrate either a current minima, or a drop to 0 nA. For approaches with sufficiently high pressures, the current reached 0 nA due to the constriction of solvent flow by the nebulizing gas. For pressures below 180 psi, there was an observable decrease in current; however, current values did not fall to 0 nA.

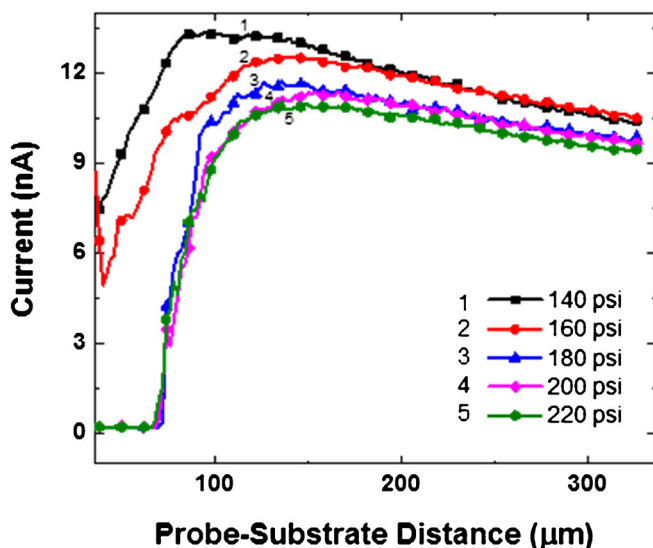


Figure 5. Approach curves taken at various nebulizing gas pressures with a 10 μm i.d. pipette at 550 V and with a constant flow rate of 0.5 μL/min

Topography and Mass Spectrometry Image of a TEM Grid

For hybrid topographic-chemical imaging, flexible, chemically-resistant, insulative tubing was chosen to transfer ions from the SESM-DESI platform to the MS inlet. Despite concerns regarding charge build-up on insulative transfer line, previous reports have demonstrated stable signal for both conventional stainless steel and insulative Tygon tubing transfer line materials [30]. Prior to image acquisition, adjustments to transfer line position were made to optimize ion signal, and the flexible nature of the Tygon tubing permitted this fine-tuning while transferring ions ~1 m away to the MS inlet.

As a proof-of-concept of SESM-DESI, rhodamine 6G was coated onto a 50 mesh TEM grid and imaged via a modified approach-retract scanning method (S-1). Grid features were determined on a bare TEM grid through use of a stylus profiler, referred to here as actual size. The MSI (Figure 6b) of the 443 m/z peak of rhodamine 6G was acquired simultaneously with the topography image (Figure 6a). Images of the substrate after experiments showed removal of rhodamine 6G (Figure 6c).

The dimensions of the grid (Figure 6a) were found to be (actual/imaged): 30–35/~40 μm bar height, 80/200–300 μm inner bar width, 530/500–600 μm inner bar spacing. While the actual and measured inner bar spacing showed good agreement, the inner bar width broadening can be attributed to the similarity in size between the pixels (100 μm) and bar width (80 μm). Inner bar heights were 5–10 μm higher than expected, which may be the result of the nebulizing gas flowing underneath, thus lifting the grid while imaging. Rhodamine 6G was observed in Figure 6b at locations that correspond to the TEM grid, as determined by topography in Figure 6a; hence, incorporation of SESM with simultaneous DESI measurement was achieved.

Summary of Parameters on Probe-Substrate Interaction

While the applied potential showed minimal influence on approach curve shape, both nebulizing gas pressure and solution flow rate could in some cases alter approach curve shape. SESM-DESI approach and retract curves (Figure 2) showed a hysteresis between where the spray current fell to 0 nA and when the spray current became non-zero upon probe retraction. The spray current hysteresis in SESM-DESI is explained by air entering the pipette when 0 nA is registered; upon retraction of the probe a small amount of time is required for the air bubble to be removed. Optical images of the spray pipette at 0 nA verified the presence of air inside the pipette. The hysteresis time can be nearly instantaneous, or in some cases a few seconds, but is consistent for a given set of parameters.

At tip protrusion distances <300 μm, air was observed to fill the entire electrospray pipette, which permanently stopped the current. At large tip protrusion distances >1 mm, air rarely entered the pipette and currents of 0 nA were rarely observed. One explanation is that at large tip protrusion distances, the nebulizing tip is farther away from the substrate, which

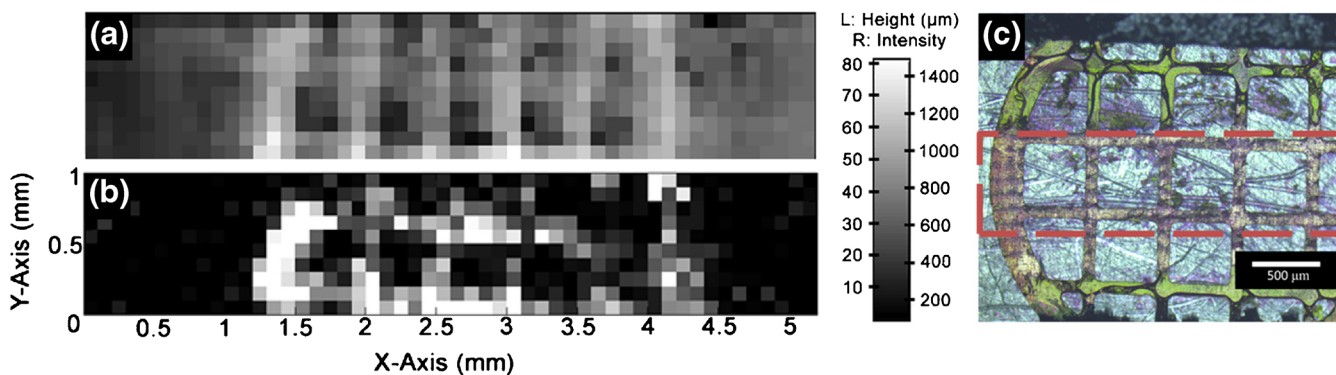


Figure 6. (a) Topography image of a 50-mesh TEM grid acquired with SESM-DESI. Image dimensions: 5.1×1.0 mm, pixel dimensions 100×100 μm . (b) Mass spectrometry image of rhodamine 6G (443 ± 0.5 m/z) measured from the top of a TEM grid. Both (a) and (b) images were acquired simultaneously with a 12 μm o.d. pipette, 500 V applied potential, 2 $\mu\text{L}/\text{min}$ solution flow rate, 160 psi nebulizing gas pressure, and 90° spray angle. The scale bar represents the sample height (left side, Figure 6a) and 443 m/z intensity (right side, Figure 6b). (c) Picture of TEM grid after imaging (imaged area shown inside the red box)

prevents the gas flow from becoming sufficiently strong to overcome the syringe pump, while at short tip protrusion distances, the gas flow can overcome solution flow into the pipette tip.

A zero-current value was necessary to produce a stable and robust feedback signal for SESM-DESI imaging. To achieve a useful feedback signal, the following parameters must be empirically tuned for a given pipette: voltage, solution flow rate, nebulizing pressure, and tip-protrusion distance. First the electro spray onset potential in the absence of nebulizing gas and infusion should be found and the potential of the pipette should be set to 100 V above the onset potential. Next, a solution flow rate of ~ 5 $\mu\text{L}/\text{min}$ can be introduced and the nebulizing gas turned to 140 psi. An approach curve can then be recorded. If the approach curve does not yield a zero current value, the approach curve should be repeated at a higher nebulizing pressure. If the range of nebulizing gas pressure has been exhausted, and the approach curve failed to yield a zero-current value, the solution flow rate should be decreased and the entire process repeated until a zero-current value is observed. If the solution flow rate has to be decreased to a point where desorption no longer occurs, the tip-protrusion distance should be altered by turning the end cap and all parameters should be retested. After the solution flow rate, nebulizing gas pressure, and tip-protrusion are tuned, voltage can then be altered to limit the current to below 30 nA during approaches.

Conclusions

DESI-MSI has been coupled to SESM to provide simultaneous topographic and chemical information. Our systematic exploration of key parameters shows that solution flow rate and nebulizing gas pressure dominate the shape of approach curves, and therefore probe-substrate interactions. In the future, synthetic surfaces, such as patterned polymers, may prove useful as training samples. While polymeric samples would prove

challenging, previous reports of DESI [31, 32] and reactive-DESI [33], which employs use of solvent additives to selectively react with analytes, have been successfully demonstrated for polymers. In addition to synthetic training samples, characterization of spatial distribution of polymeric excipients in pharmaceutical samples would be uniquely served by DESI-analysis, when the active pharmaceutical ingredient is prone to degradation by more energetic means of characterization. Through careful tuning of the parameters, a highly reproducible probe-substrate distance relationship can be achieved with SESM-DESI.

Acknowledgments

Financial support was provided by Indiana University. The authors recognize the Indiana University Electronic Instrument Services and Mechanical Instrument Services, in particular Mr. Bruce Frye, for aid in fabrication. The Nanoscale Characterization Facility at Indiana University is recognized for use of the stylus profiler.

References

1. Takáts, Z., Wiseman, J.M., Gologan, B., Cooks, R.G.: Mass spectrometry sampling under ambient conditions with desorption electrospray ionization. *Science*. **306**, 471–473 (2004)
2. Cooks, R.G., Ouyang, Z., Takáts, Z., Wiseman, J.M.: Ambient mass spectrometry. *Science*. **311**, 1566–1570 (2006)
3. Venter, A., Sojka, P.E., Cooks, R.G.: Droplet dynamics and ionization mechanisms in desorption electrospray ionization mass spectrometry. *Anal. Chem.* **78**, 8549–8555 (2006)
4. Costa, A.B., Cooks, R.G.: Simulation of atmospheric transport and droplet-thin film collisions in desorption electrospray ionization. *Chem. Commun.* **38**, 3915–3917 (2007)
5. Iribarne, J.V., Thomson, B.A.: On the evaporation of small ions from charged droplets. *J. Chem. Phys.* **64**, 2287–2294 (1976)
6. Ahadi, E., Konermann, L.: Ejection of solvated ions from electrosprayed methanol/water nanodroplets studied by molecular dynamics simulations. *J. Am. Chem. Soc.* **133**, 9354–9363 (2011)

7. Dole, M., Mack, L.L., Hines, R.L., Mobley, R.C., Ferguson, L.D., Alice, M.B.: Molecular beams of macroions. *J. Chem. Phys.* **49**, 2240–2249 (1968)
8. Winger, B.E., Light-Wahl, K.J., Ogorzalek Loo, R.R., Udseth, H.R., Smith, R.D.: Observation and implications of high mass-to-charge ratios from electrospray ionization mass spectrometry. *J. Am. Soc. Mass Spectrom.* **4**, 536–545 (1993)
9. Ahadi, E., Konermann, L.: Modeling the behavior of coarse-grained polymer chains in charged water droplets: implications for the mechanism of electrospray ionization. *J. Phys. Chem. B.* **116**, 104–112 (2012)
10. Chung, J.K., Consta, S.: Release Mechanisms of poly(ethylene glycol) macroions from aqueous charged nanodroplets. *J. Phys. Chem. B.* **116**, 5777–5785 (2012)
11. Konermann, L., Rodriguez, A.D., Liu, J.: On the formation of highly charged gaseous ions from unfolded proteins by electrospray ionization. *Anal. Chem.* **84**, 6798–6804 (2012)
12. Konermann, L., Ahadi, E., Rodriguez, A.D., Vahidi, S.: Unraveling the mechanism of electrospray ionization. *Anal. Chem.* **85**, 2–9 (2013)
13. Nguyen, S.N., Liyu, A.V., Chu, R.K., Anderton, C.R., Laskin, J.: Constant-distance mode nanospray desorption electrospray ionization mass spectrometry imaging of biological samples with complex topography. *Anal. Chem.* **89**, 1131–1137 (2017)
14. Roach, P.J., Laskin, J., Laskin, A.: Nanospray desorption electrospray ionization: an ambient method for liquid-extraction surface sampling in mass spectrometry. *Analyst.* **135**, 2233–2236 (2010)
15. Yuill, E.M., Shi, W., Poehlman, J., Baker, L.A.: Scanning electrospray microscopy with nanopipets. *Anal. Chem.* **87**, 11182–11186 (2015)
16. Ushiki, T., Nakajima, M., Choi, M., Cho, S.-J., Iwata, F.: Scanning ion conductance microscopy for imaging biological samples in liquid: a comparative study with atomic force microscopy and scanning electron microscopy. *Micron.* **43**, 1390–1398 (2012)
17. Ovchinnikova, O.S., Kjoller, K., Hurst, G.B., Pelletier, D.A., Van Berkel, G.J.: Atomic force microscope controlled topographical imaging and proximal probe thermal desorption/ionization mass spectrometry imaging. *Anal. Chem.* **86**, 1083–1090 (2014)
18. Ovchinnikova, O.S., Nikiforov, M.P., Bradshaw, J.A., Jesse, S., Van Berkel, G.J.: Combined atomic force microscope-based topographical imaging and nanometer-scale resolved proximal probe thermal desorption/electrospray ionization-mass spectrometry. *ACS Nano.* **5**, 5526–5531 (2011)
19. Kertesz, V., Van Berkel, G.J.: Scanning and surface alignment considerations in chemical imaging with desorption electrospray mass spectrometry. *Anal. Chem.* **80**, 1027–1032 (2008)
20. Ebejer, N., Schnippering, M., Colburn, A.W., Edwards, M.A., Unwin, P.R.: Localized high resolution electrochemistry and multifunctional imaging: scanning electrochemical cell microscopy. *Anal. Chem.* **82**, 9141–9145 (2010)
21. Chambers, M.C., Maclean, B., Burke, R., Amodei, D., Ruderman, D.L., Neumann, S., Gatto, L., Fischer, B., Pratt, B., Egertson, J., Hoff, K., Kessner, D., Tasman, N., Shulman, N., Frewen, B., Baker, T.A., Brusniak, M.-Y., Paulse, C., Creasy, D., Flashner, L., Kani, K., Moulding, C., Seymour, S.L., Nuwaysir, L.M., Lefebvre, B., Kuhlmann, F., Roark, J., Rainer, P., Detlev, S., Hemenway, T., Huhmer, A., Langridge, J., Connolly, B., Chadick, T., Holly, K., Eckels, J., Deutsch, E.W., Moritz, R.L., Katz, J.E., Agus, D.B., MacCoss, M., Tabb, D.L., Mallick, P.: A cross-platform toolkit for mass spectrometry and proteomics. *Nat. Biotech.* **30**, 918–920 (2012)
22. Race, A.M., Styles, I.B., Bunch, J.: Inclusive sharing of mass spectrometry imaging data requires a converter for all. *J. Proteom.* **75**, 5111–5112 (2012)
23. Robichaud, G., Garrard, K.P., Barry, J.A., Muddiman, D.C.: MSiReader: an open-source interface to view and analyze high resolving power MS imaging files on Matlab platform. *J. Am. Soc. Mass Spectrom.* **24**, 718–721 (2013)
24. Hendricks, J.C.D., Pfeifer, R.J.: Parametric studies of electrohydrodynamic spraying. *AIAA J.* **6**, 496–502 (1968)
25. Eyring, C.F., Mackeown, S.S., Millikan, R.A.: Fields currents from points. *Phys. Rev.* **31**, 900–909 (1928)
26. Jones, A.R., Thong, K.C.: Production of charged monodisperse fuel droplets by electrical dispersion. *J. Phys. D – Appl. Phys.* **4**, 1159 (1971)
27. Smith, D.P.H.: The electrohydrodynamic atomization of liquids. *IEEE Trans. Ind. Appl.* **22**, 527–535 (1986)
28. Venter, A., Cooks, R.G.: Desorption electrospray ionization in a small pressure-tight enclosure. *Anal. Chem.* **79**, 6398–6403 (2007)
29. Takáts, Z., Wiseman, J.M., Gologan, B., Cooks, R.G.: Electrosonic spray ionization. A gentle technique for generating folded proteins and protein complexes in the gas phase and for studying ion–molecule reactions at atmospheric pressure. *Anal. Chem.* **76**, 4050–4058 (2004)
30. Garimella, S., Xu, W., Huang, G., Harper, J.D., Cooks, R.G., Ouyang, Z.: Gas-flow assisted ion transfer for mass spectrometry. *J. Mass Spectrom.* **47**, 201–207 (2012)
31. Jackson, A.T., Williams, J.P., Scrivens, J.H.: Desorption electrospray ionisation mass spectrometry and tandem mass spectrometry of low molecular weight synthetic polymers. *Rapid Commun. Mass Spectrom.* **20**, 2717–2727 (2006)
32. Nefliu, M., Venter, A., Cooks, R.G.: Desorption electrospray ionization and electrosonic spray ionization for solid- and solution-phase analysis of industrial polymers. *Chem. Commun.* **8**, 888–890 (2006)
33. Nefliu, M., Cooks, R.G., Moore, C.: Enhanced desorption ionization using oxidizing electrosprays. *J. Am. Soc. Mass Spectrom.* **17**, 1091–1095 (2006)